, ,
Draft version July 30, 2022
Typeset using LaTeX **manuscript** style in AASTeX631

Orbital Determination of 1994 PC1 by the Method of Gauss

C. Wilk,[1] E. Kuperman,[1] and K. Nabi[1]

[1]*Summer Science Program and Sommers-Bausch Observatory, University of Colorado Boulder, Boulder, CO, 80309, USA*

(Received July 22, 2022; Revised July 30, 2022; Accepted July 27, 2022)

ABSTRACT

This study determines the orbital elements of the Apollo group near-Earth asteroid 1994 PC1 through an iterative computation transformation of position and velocity vectors and Monte Carlo simulation. These processes stem from novel imaging in the visual wavelengths and computerized catalog astrometry. We find, based on three successive observation dates, a semi-major axis length of 1.352 AU, an eccentricity of 0.334, an inclination angle of 33.415 degrees, an argument of perihelion of 47.740 degrees, a mean anomaly of 74.165 degrees, a longitude of ascending node of 117.892 degrees, and a time of perihelion passage of 2459637.414 days based on six probability distributions. We present Gaussian densities for each value besides the time of perihelion passage. Consequently, these elements can be derived from user-controlled position and velocity vector inputs to pinpoint 1994 PC1's RA and Dec both in the past and future, on timescales of decades to centuries. We perform an examination of the RA and Dec on the time of the third observation and return inconsequential errors for verification; namely, the RA lies within 0.00048% of NASA JPL Horizons' value and the Dec within 0.064%. Furthermore, through photometric reference star regressions, we determine an average magnitude of 17.0 V for analyses across nine time-separated light frame images.

1. INTRODUCTION

The Solar System hosts many types of debris, ranging from offloaded space junk to comets and asteroids. As a collective, this debris plays an important role in Solar System dynamics and also requires modeling as a forecast for orbit perturbation within the debris collective and a safeguard for impact with Earth. Among these candidates, potentially hazardous near-Earth asteroids (NEAs) have long been considered in solar system astrophysics as both high-priority motivations for planetary defense and candidates for potential flybys (Balkoski et al. 2011 (1), Foster and Daniels 2010 (2)). While the heavily elliptical orbit of icy comets may bring them to near approaches, asteroids are more numerous and less understood. In fact, as of 2021, only 0.5 percent of near-Earth asteroids had been tracked, according to the Asteroid Institute of the B612 Foundation (Posner 2020 (3)). The orbits of such objects, therefore, remain open questions in solar system astrophysics and benefit greatly from frequent calculation (Bowell et al. 2002 (4)).

Near-Earth asteroid search campaigns are often employed to better understand these objects, which exist in four main groups. Atira asteroids have aphelions interior to earth's orbit, Aten asteroids have semi-major axes measuring less than 1 AU with aphelions interior to Earth's perihelion, Apollo asteroids have semi-major axes greater than 1 AU with perihelions interior to Earth's aphelion, and Amor asteroids always orbit outside Earth's orbit but may cross Mars' orbit. Of these groups, both Aten and Apollo asteroids cross Earth's orbit. Although asteroid search campaigns are intrinsically useful for planetary defense, they also raise awareness of astronomy and result in new discoveries. Various methods and recent modules, including algorithms of Gauss and Laplace as well as automated computation systems, are aptly employed to discovered asteroids to return orbital elements for orbital determination (Solin and Granvik 2018 (5)).

This paper determines the orbital trajectory of 1994 PC1, an Apollo group NEA, by using the Method of Gauss to solve for orbital state vectors and elements. These elements include the semi-major axis (a), eccentricity (e), inclination (i), argument of perihelion (ω), mean anomaly (M), longitude of ascending node (Ω), and time of perihelion passage (T). a is the distance, conventionally in AU, of one-half of an elliptical orbit's greater axis. e is a dimensionless quantity that represents

the degree to which the orbit is elliptical, ranging from zero to one. i is the angle between the plane of the elliptical orbit and the plane of the solar system, or the ecliptic. ω represents the angle between the asteroid's perihelion and the ascending node on the line of nodes where the orbital plane and the ecliptic intersect. M is the portion of the asteroid's period elapsed since its most recent perihelion passage. Ω is the angle from the vernal equinox to the ascending node in the ecliptic plane. Lastly, T is the time in Julian days since the asteroid last passed its perihelion. The astrometric and photometric data in this work are based on novel digital imaging using the Sommers-Bausch Observatory's Artemis East Planewave telescope. In obtaining 1994 PC1's ephemeris, this study comprises usages of distance moduli, Newtonian mechanics including the Theory of Gravitation, and the Gaussian formulation of Kepler's laws of planetary motion. In determining the final ephemeris values, Monte Carlo simulation is employed to generate normalized probability distributions of each respective element.

2. OBSERVATIONS AND IMAGE PROCESSING

2.1. *Data Acquisition*

Each of three observations, on 6/23/2022, 6/25/2022, and 7/17/2022, was conducted using the Sommers-Bausch Observatory's East Planewave instrument. NASA JPL Horizons application was used in order to acquire an ephemeris table for 1994 PC1, specifically the RA and Dec used to locate 1994 PC1 at 15-minute time intervals. In addition, a DS9 star chart based on the RA and Dec was used reference material and to confirm the asteroid's position qualitatively during observation. During every observation, 1994 PC1 was found both in a series of images and on the star chart.

As a data acquisition tool, we used a Corrected Dall-Kirkham (CDK) 20" telescope which produces no off-axis coma and no off-axis astigmatism, has an f/6.8 aperture and 3454mm focal length, and is capable of locating stars across a 52mm image circle. TheSkyX Software, with integrated astronomical databases for object identification, was used to locate and identify 1994 PC1. By using TheSkyX, the telescope and camera were controlled synchronously through automatic computer commands. All observations were taken with the STF-8300 with a KAF-8300 CCD and a 20-inch mirror. This

camera and filter are automatically connected to TheSkyX. Each observation used the UV/IR cutoff (L) filter with 2x2 binning to observe in visual wavelengths with a consistent temperature near -5°C using no more than 80% power. The telescope was slewed to RA and Dec values determined from the NASA JPL Horizons ephemeris table. After confirming the presence of 1994 PC1 with a test light image and matching the star field in the image with the computer-generated star chart, light images were taken in series of three, separated by about ten minutes with a 40-second exposure time to ensure visibility. Five to ten dark frame images were taken with the same settings as the light frames in between ten minute intermediate intervals.

This process was repeated for three observation sessions which are briefly recorded below in Table 1. The observation sessions are well spaced but not even, despite precision generally increasing with equidistant spacing, simply because of telescope scheduling and natural observing constraints.

Table 1: Three observations of 1994 PC1 using the time of the middle light image, with notes.

Location of Observatory	Date	Time	More Information
Sommers-Bausch Observatory (463)	June 23, 2022	06:39:17.185	Clear conditions, minimal cloud cover
Sommers-Bausch Observatory (463)	June 25, 2022	06:26:01.024	Clear conditions, no cloud cover
Sommers-Bausch Observatory (463)	July 17, 2022	06:23:56.348	Clear conditions with strong moonlight

2.2. *Image Reduction, Astrometry, and Photometry Methods*

AstroImageJ (AIJ), a version of ImageJ with integrated astrophysics macros, was used in the process of flat and dark reduction, astrometry, and calibrated photometry. Dark and flat images were compiled into master files which were then applied to three sets of three lights each per day to obtain high-resolution images with identifiable, coordinate-sorted objects. Each dark image was taken at the site immediately after three sets of lights. Flat images were taken on each night of The middle image of each set was then uploaded to nova.astrometry.net, an online astrometric solver calibrated to the USNO-B catalog, and then the astrometry-corrected images were downloaded and displayed in AIJ. Sets of RA and Dec for 1994 PC1 were determined for each of the three stacked images at the time stamp of the midpoint of the applicable observation.

Photometric data of the astrometry-corrected images was compiled via SAOImage DS9 using RA and DEC-tagged images to the nearest second of observation. The magnitudes of three reference stars within the field of view of the image are determined using AAVSO APASS. AIJ was used in conjunction with DS9 to obtain peak values in ADU. For this study, the peak threshold was held at 30,000 ADU for reference stars. Additional values, namely the source-sky and RA and Dec of each star, were also recorded in AIJ after location and V extraction from DS9. Based on the magnitudes and their corresponding source-sky, asteroid magnitudes for midpoint exposure time realizations were determined from the canonical modulus,

$$V = -2.5\log(S) + (y - mx) \tag{1}$$

where the intercept is taken from a regression with an approximate slope of (-2.5) using the three reference stars.

2.3. *Astrometric Error Determination*

To determine the RA and Dec of the asteroid, the raw images taken from the telescope were uploaded to nova.astrometry.net and analyzed using least squares plate reduction (LSPR). This method requires determining the x and y coordinates of the asteroid, the x and y coordinates of n reference stars, as well as the RA and Dec of each star. Then by applying Cramer's rule, the RA and Dec of the asteroid are calculated, along with the their respective uncertainties. These values were downloaded from nova.astrometry.net and the root mean square for the uncertainties was calculated for the middle series of each observation. The RA and Dec of the asteroid and their associated uncertainties are displayed in Table 2.

2.4. *Results*

In this paper, RA and Dec will be reported to the number of places suggested by the International Astronomical Union Minor Planet Center (former seconds to two decimal places, latter seconds to one decimal place). While three individual images were used to determine the orbital elements of 1994 PC1, RA and Dec values were acquired from image analysis for nine different times, three per

date (6/23/2022, 6/25/2022, and 7/17/2022). Table 2 lists each RA and Dec pair with a companion time in UTC.

Table 2: RA and Dec for 1994 PC1 from nine images.

Date and Time	RA (J2000), h:m:s	Dec (J2000), deg:m:s
6/23.26758	19:55:01.57	+15:53:11.7
6/23.27728	**19:55:00.15** $\pm$ 3.549$\times$ 10^{-5}	**+15:52:41.6** $\pm$ 2.956$\times$ 10^{-5}
6/23.28599	19:54:58.89	+15:52:14.8
6/25.25925	19:50:16.81	+14:07:04.4
6/25.26807	**19:50:15.36** $\pm$ 2.696$\times$ 10^{-5}	**+14:06:42.1** $\pm$ 3.026$\times$ 10^{-5}
6/25.27502	19:50:14.54	+14:06:30.9
7/17.26161	18:54:59.77	- 08:53:18.0
7/17.26662	**18:54:59.04** $\pm$ 3.752$\times$ 10^{-5}	**- 08:53:36.6** $\pm$ 2.378$\times$ 10^{-5}
7/17.27315	18:54:58.20	- 08:54:00.8

Bold items were used in the orbital determination procedure, as they formed the middle image of the middle set of each observation.

In a similar fashion, magnitudes are listed in Table 3. See A2 for a sample graph demonstrating the regression applied to a series of reference stars. Across all observations, the unweighted average magnitude of 1994 PC1 was 17.0 V while NASA JPL Horizons gives a magnitude of 16.58 V, resulting in a truncated percent error of 2.5%. Although asteroids emit most of their light in the visual wavelengths, the amount of light that reaches the earth is variable (National Academies of Sciences, Engineering, and Medicine 2019 (6)). Although measuring luminosity peaks and troughs is beyond the scope of this paper, it is possible that this discrepancy is due to alternating brightness based on position and orientation.

Table 3: 1994 PC1's apparent V magnitudes across nine observations.

Date and Time	V Magnitude
6/23.26758	16.9
6/23.27728	**17.3**
6/23.28599	17.0
6/25.25925	17.2
6/25.26807	**16.9**
6/25.27502	16.8
7/17.26161	16.9
7/17.26662	**16.8**
7/17.27315	17.2

3. ORBIT DETERMINATION

3.1. *Methods*

The Method of Gauss, an iterative celestial mechanics algorithm, was performed on three sets of RA (J2000) and Dec (J2000) acquired during the midpoint of each central 40 second exposure on the aforementioned dates. See Table 1 for exact times per date. The method described below was written and executed in Python 3.0 using a series of successive functions designed for orbital determination.

Initial values for D-matrices, components of equations of range used to derive $\vec{\rho_i}$ values, were computed by indexing the RA and Dec pairs within each midpoint set. The directional velocity vectors $\hat{\rho_i}$ were simultaneously derived by necessity, as the D-matrices are dependent on both the Sun-Earth vectors at each time of observation and three $\vec{\rho_i}$ corresponding to these times. Using trigonometry in the celestial sphere and taking RA and Dec as inputs for their respective dates,

$$\hat{\rho_i} = \vec{\rho_i} \; / \; \left(\frac{C_1 D_{i1} + C_2 D_{i2} + C_3 D_{i3}}{C_i D_0} \right) = \left((sin(\alpha) \cdot cos(\delta))^2 + (sin(\alpha) \cdot cos(\delta))^2 + sin(\delta)^2 \right)^{\frac{1}{2}} \qquad (2)$$

While they are referenced here preemptively for context, the C_i factors are determined later from time-dependent constituents of the orbital vectors (Eq. 4) and recalculated through a loop. Regardless, the result is a set of three new unit vectors (which can also be obtained during iteration, discussed later, by the Scalar Equation of Range). The $\hat{\rho}_i$ vector derived from celestial coordinates at the midpoint of the second observation (RA: 19:50:15.36, Dec: 14:06:42.1) was the implemented into the Scalar Equation of Lagrange, an eighth-order polynomial intermediate step in determining 1994 PC1's initial position and velocity vectors

$$0 = r_2^8 + ar_2^6 + br_2^3 + c \tag{3}$$

where a, b, and c are dependent on ρ_2, $\hat{\rho_2}$, the middle observation Sun-Earth vector $\vec{R}_2$, and a set of time differences τ_i derived from t_i in Julian days (one per observation) and the Gaussian gravitational constant k which serves the same function as G. τ_i and τ are treated as differences of two times multiplied by k such that when $i = 1$, t_1 and t_2 are operated on, while when $i = 3$, t_3 and t_2 are instead. For the general τ the entire time difference is used. After the first iteration through the Method of Gauss, t_i was corrected for light travel time by subtracting the quotient of ρ_i and c.

RA and Dec pairs were also used to construct f_i and g_i from the Taylor Series pair

$$f_i = 1 - \frac{\tau_i^2}{2r_2^3} + \frac{\vec{r_2} \cdot \dot{\vec{r_2}}}{2r_2^5}\tau_i^3 + ... \text{ and } g_i = \tau_i - \frac{\tau_i^3}{6r_2^3} + ... \text{ for } i = 1, 3 \tag{4}$$

which function as close approximations for input into respective C_1 and C_3 equations. The iterative orbital determination code used in this study took each series to the fourth order with solutions for u, z, and q substituted according to the Boulet formulation as in A1 (Boulet 1991 (7)). For the first iteration, $\dot{\vec{r}}$ was treated as zero and as such the formulae were taken to the second order.

In determining the fractions which reduce to C_1, C_2, and C_3, pre-r-vector factors taken in to determine $\vec{r_2}$, the values for f and g were recalculated until a break at $B_{crit} = 10^{-12}$ using updated light-corrected times, τ_i values derived from these times, and ρ_i values computed from the Scalar Equation of Range (1). After iteration and retention of both a $\vec{r_2}$ and a $\dot{\vec{r_2}}$, a reversed x-rotation matrix of the general form was used to perform a transformation from the orbital plane to the ecliptic.

In this case, the orbital plane acts as a post-rotation space while the ecliptic is the original plane, thus the need for reversal.

With both the middle position and velocity vector determined, the orbital elements can be calculated through a series of successive functions of $\vec{r_2}$ and $\dot{\vec{r_2}}$, taking the velocity vector as v and $\mu = 1$. The formulae necessary to compute each orbital element are given below, in the order that they were used. Notably, a quadrant check was performed for both U, the angle between the line of nodes and $\vec{r_2}$, as well as v, the true anomaly. h, 1994 PC1's specific angular momentum, is equivalent to the cross product between its position and velocity. Resultant values are listed in Section 3.2.

$$a = \left(\frac{2}{r} - \frac{v^2}{\mu}\right)^{-1} \tag{5}$$

$$e = \sqrt{1 - \frac{h^2}{a\mu}} \tag{6}$$

$$i = \cos^{-1}\left(\frac{h_z}{h}\right) \tag{7}$$

For inclination, an alternative arc-tangent formulation also exists. This formula, which relies on all three components of h, was not used in orbital determination. Error propagation can be bountiful after calculation of i which is why the aforementioned iteration threshold was selected.

$$\Omega = \sin^{-1}\left(\frac{h_x}{h\sin i}\right) = \cos^{-1}\left(\frac{-h_y}{h\sin i}\right) \tag{8}$$

$$\omega = U - \nu \text{ for which } U = \sin^{-1}\left(\frac{z}{r\sin i}\right) = \cos^{-1}\left(\frac{x\cos\Omega + y\sin\Omega}{r}\right) \tag{9}$$

$$\text{and } \nu = \cos^{-1}\left(e^{-1}\left(\frac{a(1-e^2)}{r}\right) - 1\right) = \sin^{-1}\left(\frac{a(1-e^2)}{he} \cdot \frac{h}{r}\right)$$

Once ν was calculated, it was used in order to derive the mean anomaly M and time of perihelion passage T. Evidently, each step of the aggregate derivation is dependent on at least one previous step.

ν is a particularly important intermediate value as it is used to determine the projected eccentric anomaly onto a circle, thus the mean anomaly and also the time of perihelion passage. For instance,

$$E = \cos^{-1}\left(\frac{e + \cos v}{1 + e\cos v}\right) = \sin^{-}1\left(\frac{r\sin v}{a\sqrt{1-e^2}}\right) \text{ and } M = E - e\sin E \tag{10}$$

$$T = t - \frac{Ma^{3/2}}{\mathrm{k}}, \; t \text{ a light corrected middle observation time} \tag{11}$$

The final orbital elements define 1994 PC1's orbit, but they apply only to the values taken in. As a result, a probabilistic Monte Carlo simulation was conducted by generating random values for the RA and Dec of the asteroid, which were then used to calculate the asteroid's orbital elements. The RA and Dec values were drawn from a Gaussian distribution with a standard deviation determined from the root mean square of the uncertainties for RA and Dec at each observation, as reported by nova.astrometry.net. The Monte Carlo method was run 10,000 times for each orbital element in order to obtain a Gaussian-like probability density with a mean value to compare to accepted values.

To verify the accuracy of the newly calculated orbital elements, we performed a prescribed ephemeris self-consistency test which predicts the RA and Dec of 1994 PC1 at 7/17/2022, 06:24:56.348 UTC, using the orbital elements from 6/25/2022, 06:26:01.024 UTC. The RA value was calculated to be 18:54:59.38, which has a percent difference of 0.00048% when compared to the experimentally determined value of 18:54:59.06. The Dec value was computed to be -8.0:53:57.4, with a percent difference of 0.064% when compared to the experimentally measured value of -8.0:53:36.8.

3.2. *Results*

Table 4 shows seven calculated orbital elements and their percent differences compared to values given by the NASA JPL Horizons Osculating Orbital Elements table. Percent difference is taken to two significant figures, and the calculated values are rounded to three decimal places. Furthermore, Figure 1 displays the outputs of computational Monte Carlo simulations as histograms for six orbital elements, a through M, with a Count-axis which measures n occurrences for a given value. The mean values were calculated and then compared to NASA JPL Horizons. The Monte Carlo simulations also serve the purpose of generating values for input into an osculating orbit diagram, Figure 2, using

the *poliastro* library simultaneously with the previously described orbital determination code. This diagram depicts 1994 PC1, albeit enlarged in orbit around the Sun. The angle of inclination of the orbital plane is not represented in this diagram.

Table 4: The orbital elements of 1994 PC1.

Element	Mean	Percent Difference (%)
Semi-major axis (a)	1.352 AU	0.28
Eccentricity (e)	0.334	1.2
Inclination (i)	33.415°	0.17
Argument of perihelion (ω)	47.740°	0.56
Mean anomaly (M)	74.165°	1.1
Longitude of ascending node (Ω)	117.892°	0.015
Time of perihelion passage (T)	2459637.414 d	3.2×10^{-5}

4. DISCUSSION

The results of 1994 PC1's orbital determination by the Method of Gauss are promising. The greatest percent difference between the calculated values and the values inherent in NASA JPL Horizons is 1.2%, for the eccentricity. The lowest error is 3.2×10^{-5}% for the time of perihelion passage. As verified by the self-consistency test, input vectors for one time can be used to determine, to near identical consistency with NASA JPL Horizons, the RA and Dec of 1994 PC1 on any future time. Although the lifetime of this determinations accuracy is finite, it can reasonably determine 1994 PC1's position for timescales on the order of thousands of years before perturbations or potential collisions alter the orbital elements. Recovering the RA and Dec confirms usability of the code. The quality of results was potentially affected in numerous ways. First of all, the Method of Gauss works best when observations used as inputs are well-spaced. Ideally, light images would be evenly spaced with time differences of multiple days. In this study, the first two observations were unusually close, separated by one solar day. While this did not affect the usability of the code and Monte Carlo distributions, error likely would be reduced if better spaced Ra and DEC values were used. Furthermore, a fourth

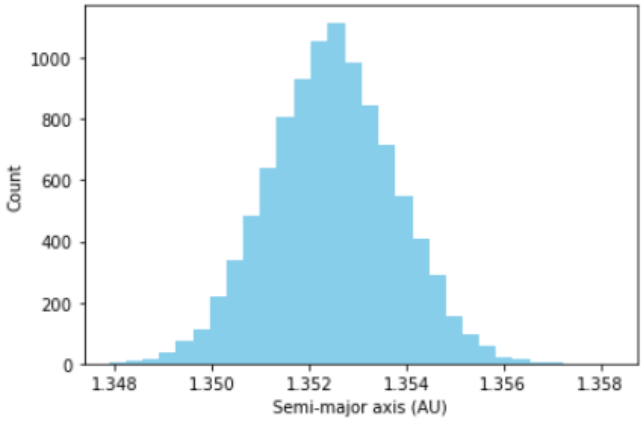

(a) Semi-major axis a

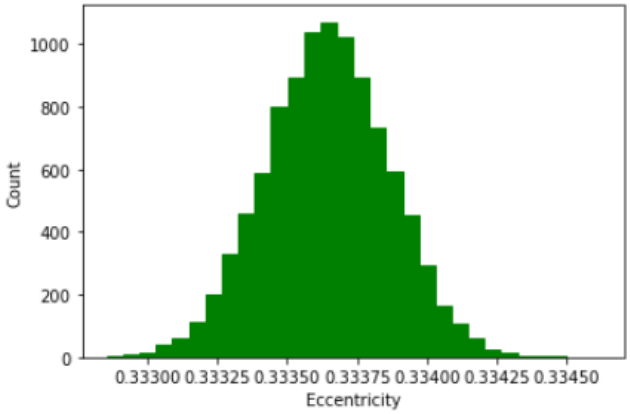

(b) Eccentricity e

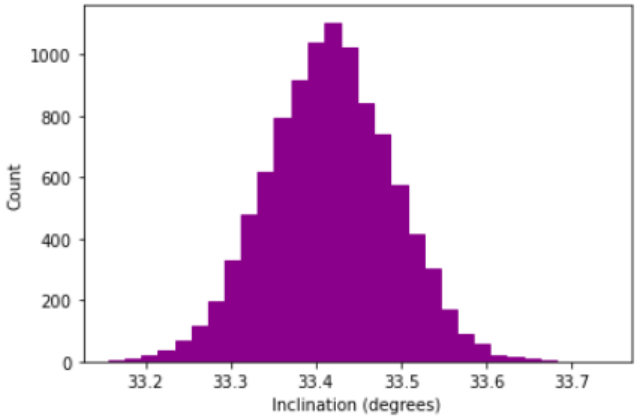

(c) Inclination i

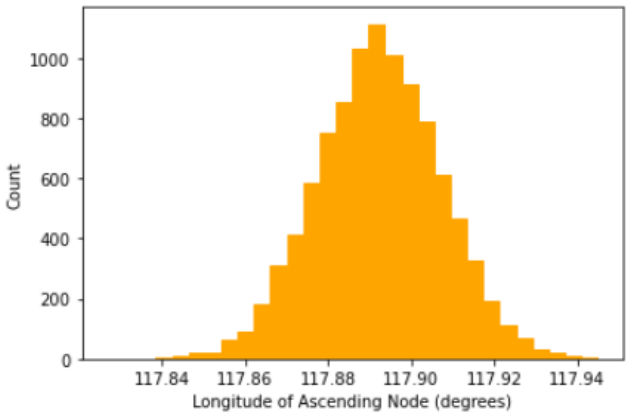

(d) Longitude of Ascending Node Ω

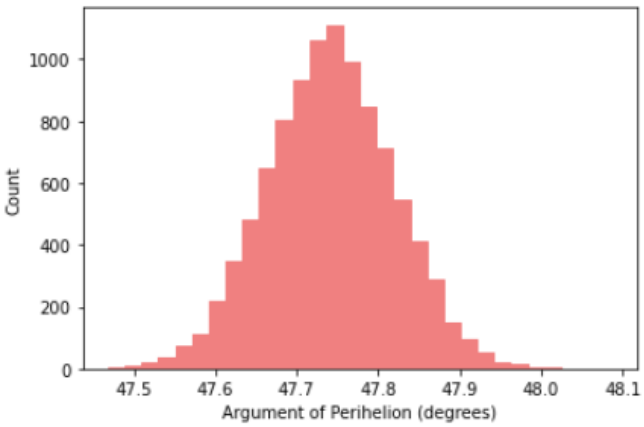

(e) Argument of Perihelion ω

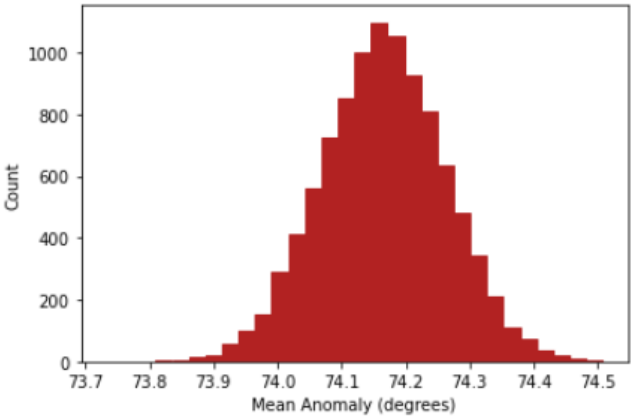

(f) Mean Anomaly M

Figure 1: Histograms for each orbital element representing the results of Monte-Carlo simulations

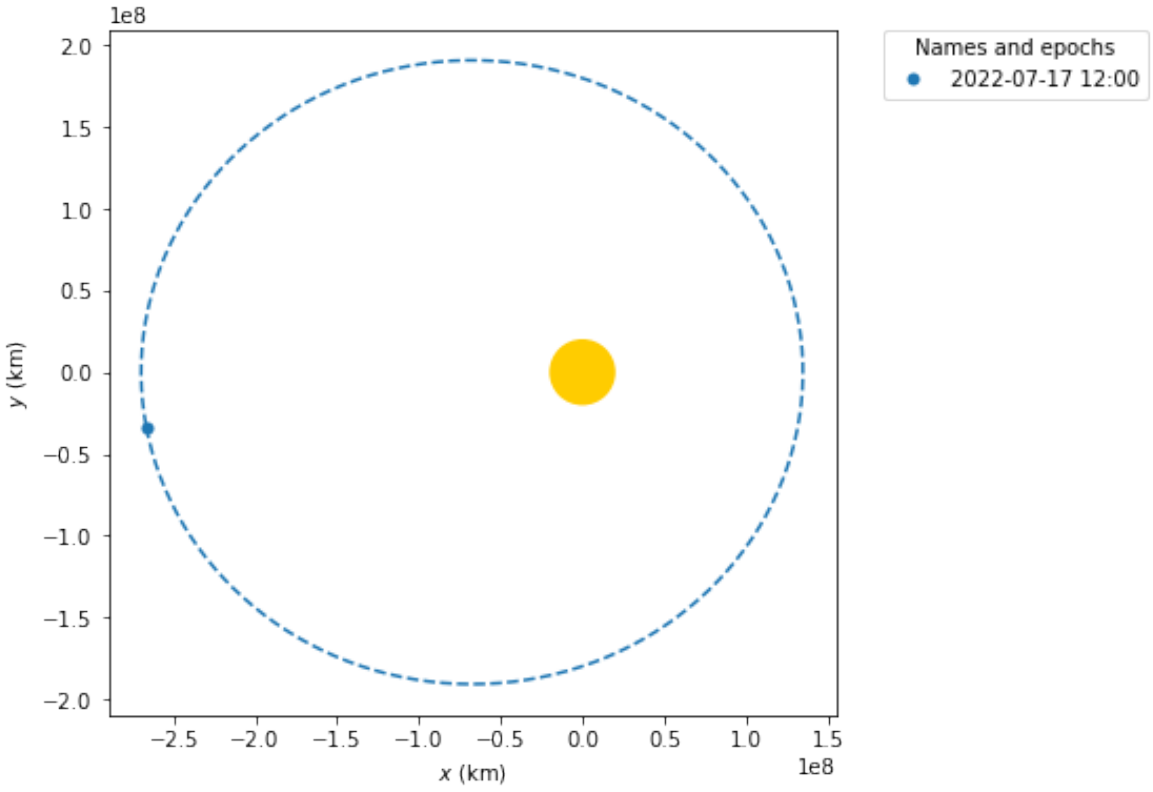

Figure 2: An element-dependent 2000 epoch osculating orbit diagram displaying 1994 PC1 as an enlarged static point on its orbital ellipse.

observation which could be used to improve the results was not included because of a satellite streak interfering with images for an unusual period of time paired with mild cloudiness. Increasing the quality of, quantity of, and separation between observations would likely bring the error of each orbital element and the final RA and Dec computed in the self-consistency test down. In this case, error refers to the difference between the computed values and the true values, which are possibly stored by the NASA JPL Horizons repository.

5. REFLECTION

During our experience working on this project, we encountered numerous challenges that seemed daunting and at times unsolvable. Such problems often originated with coding assignments, but when broken down into bits and pieces, when taken line by line, the solution would start to unravel. We all feel that this experience was truly rewarding not only because we were able to complete a remark-

able project but because we realize how much we have strengthened our abilities to problem-solve, collaborate, and appreciate science. The demand for this project paved the path for us to become much more adept researchers, increasing our self-motivation and awareness of our own strengths and weaknesses.

We particularly enjoyed the nights of observations in the Sommers-Bausch Observatory. Operating the telescope, processing images of 1994 PC1, and gazing at stellar celestial bodies made each night on the observatory deck memorable. Although we knew that these observation times would be followed by dreadfully long hours working on photometry, we consistently worked together as a team to ensure that everyone was able to complete their work on time. When these seemingly impossible challenges are overcome by rewarding collaboration is when research, however serious, becomes fun.

The division of labor was based on each of our strong suits, although we often all worked together on projects simultaneously. Within our group, we have a diverse range of expertise. While each of us made various contributions, each member was able to assist collaborators with their areas of strength and to blossom in their areas of weakness. During this project, we all experienced collective struggles and mutual growth. Certainly, this project has inspired us to both learn and engage in science in the future.

6. ACKNOWLEDGEMENTS

We would like to thank Dr. Donovan Domingue (Georgia College and State University), Dr. Michael Dubson (University of Colorado Boulder), Jessica Dong (Massachusetts Institute of Technology), Grace Edwards (University of Colorado Boulder), Peter Lande (University of Colorado Boulder), and Mia Liang (Wesleyan University), for motivating this study and offering useful guidance. We also greatly appreciate the facilities that the University of Colorado Boulder provided for this research and are very thankful to the Summer Science Program, California Institute of Technology, Harvey Mudd College, and Massachusetts Institute of Technology for making this experience possible for us.

REFERENCES

[1]Balkoski, S. J., Bhasin, L., & Wang, M. 2011, arXiv: 1111.5283

[2]Foster, C. & Daniels, M 2010, AIAA Space 2012, AIAA Conference Exposition, 8609-1

[3]Posner, A., 2020, Asteroid 2018 VP1 – So Close, Yet So Far Away, v1.0, B612 Foundation

[4]Bowell E., Virtanen J., Muinonen K., & Boattini A. 2002, USRA Pub., 27

[5]Solin, O. & Gravnik, M. 2018, AA, 616, 176

[6]National Academies of Sciences, Engineering, and Medicine 2019, Finding Hazardous Asteroids Using Infrared and Visible Wavelength Telescopes, (1st ed.; Washington, DC: The National Academies Press) https://doi.org/10.17226/25476

[7]Boulet, D. 1991, Methods of Orbit Determination for the Microcomputer, (1st ed.; Richmond:, VA: Willmann-Bell)

7. APPENDIX

A1: The Boulet formulation for f_i and g_i series uses u, q, and z in both series to allow for computational ease and documentation. The values of each factor are found prior to executing the initial f_i and g_i series and also the iterative sequence.

$$\dddot{\vec{r}} = (3uq - 15uz^2 + u^2)\vec{r_2} + 6uz\dot{\vec{r_2}}, \tag{12}$$

$$u = \frac{1}{r_2^3} = (\vec{r_2} \cdot \vec{r_2}) - q, \tag{13}$$

$$z = \frac{\vec{r_2} \cdot \dot{\vec{r_2}}}{r^2} \tag{14}$$

A2: A reference graph (Figure 3) displaying the distance modulus dependent on signals from three reference stars per set. This regression returns a V-magnitude of 7.19. See Section 2.4 for a full listing of magnitude regression results, all of which were determined using this method.

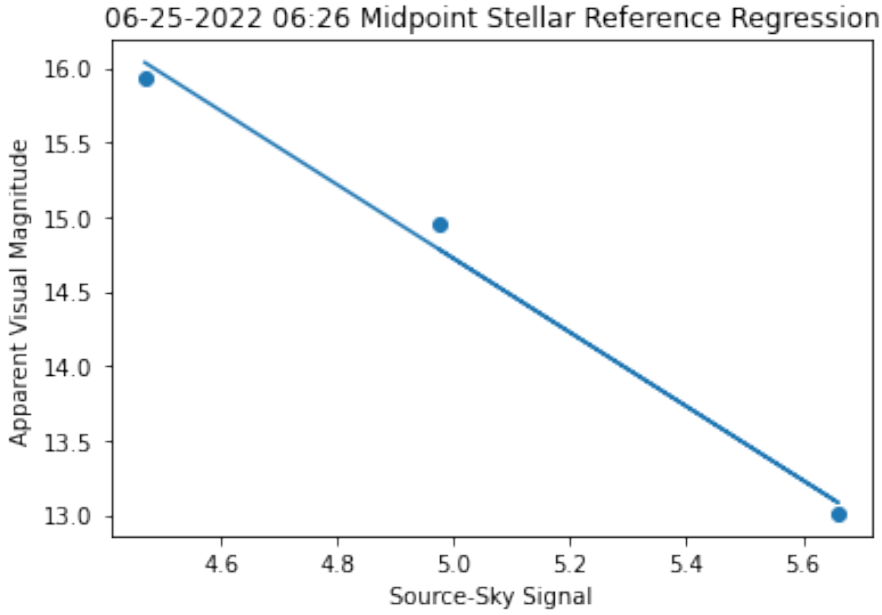

Figure 3: A magnitude regression for the midpoint image of the middle day which shows a near-linear relationship for three stars in the same field as 1994 PC1 (A2).